Low and high frequency oscillations of the accelerating electric field in a Hall thruster

IEPC-2013-089

Presented at the 33rd International Electric Propulsion Conference,
The George Washington University, Washington, D.C., USA
October 6–10, 2013

J. Vaudolon*, B. Khiar† and S. Mazouffre‡
CNRS - ICARE (Institut de Combustion, Aerothermique, Reactivite et Environnement)
1C, Avenue de la Recherche Scientifique, 45071 Orleans Cedex 2, France

The performances of Hall thrusters are greatly influenced by the discharge current oscillations. In order to characterize the oscillations of the plasma parameters, we measured the time-resolved Xe^{+} ion velocity distribution function in the discharge and the near-field plume of a low power permanent magnets Hall thruster. The distribution functions are obtained by means of a time-resolved laser-induced fluorescence technique based on a photon counting method, while time coherence is ensured by applying a sinusoidal potential modulation on a floating electrode located in the plasma. The measurements are therefore local, non intrusive and the temporal resolution is 100 ns. The discharge oscillations are consistent with those of a standard operating point. The oscillations of the electric field along the thruster discharge channel are computed. Results indicate that the electric field is mainly oscillating outside the channel. The oscillation frequencies range from the kHz up to the ion plasma frequency. The high frequency discharge oscillations are shown to be stabilized by the low frequency oscillations.

Nomenclature

h	= channel width
d	= channel mean diameter
r	= radial direction
θ	= azimuthal direction
z	= channel axis
m_i	= Xe^{+} ion mass
m_e	= electron mass
e	= elementary charge
k	= Boltzmann constant
n	= plasma density
$v,\ V$	= velocity
E	= electric field
B	= magnetic field
U_{acc}	= accelerating voltage
$<>$	= time-averaged quantity

*Ph.D. student, Electric Propulsion Team, julien.vaudolon@cnrs-orleans.fr
†Undergraduate student, Electric Propulsion Team
‡Research Scientist, Electric Propulsion Team Leader, stephane.mazouffre@cnrs-orleans.fr

I. Introduction

In the field of space propulsion, the necessity to perform various missions requires versatile thrusters, high reliability and performance. Electric propulsion has the benefit of a low propellant consumption and a significant thrust to power ratio resulting in mass and cost savings compared to chemical propulsion. Plasma propulsion is mostly dedicated to high ΔV manoeuvres such as station keeping and orbit topping for communication satellites. In a very near future, this technology will be used to realize full orbit transfers and interplanetary journeys. Despite decades of research on Hall thrusters, the physics at play is far from being fully understood. Careful experiments are therefore needed by engineers and by numerical simulations for their outcome validation.
Hall thrusters are cross-field discharges that ionize a gas to generate thrust [1, 2]. Xe is usually used owing to its low ionization potential and its high atomic mass. A radial magnetic field traps part of the electrons emitted from an external hollow cathode. The low electron conductivity generates an axially-directed electric field that accelerates the unmagnetized ions outside the thruster channel. It is well known, and it has been reported in numerous studies, that the discharge of a Hall thruster is highly non stationary. Plasma fluctuations encompass many kinds of physical phenomena [3]. A better knowledge of the discharge instabilities is necessary in order to improve the performance and the lifetime of these thrusters as they play a major role on ionization and transport processes.
In these devices, the electric field is at the origin of the Hall current responsible for the efficient ionization of the gas. In addition it accelerates the ions to generate thrust. It is therefore a fundamental quantity that can be used to describe ionization and acceleration. The most common way to measure the time evolution of the electric field in a Hall thruster is to use a fast-moving emissive probe and to differentiate the plasma potential to obtain the electric field. However, this technique is intrusive and strongly disturbs the discharge [4]. Instead, an optical method can be used. Mazouffre and Bourgeois studied the spatio-temporal characteristics of several ion velocity groups in the plume of a PPS 100-ML Hall thruster using time-resolved laser-induced fluorescence (TR-LIF) on metastable Xe^+ ions [5]. As detailed in the paper, there is the necessity to accumulate photons over several oscillation periods. The time coherence was ensured by using a fast power switch which perodically switched off the anode current during 10 μs. The time-resolved electric field was measured under these conditions, but the time-averaged discharge behavior was strongly perturbed by this system. A recent control technique of the discharge oscillations has been successfully used to perform TR-LIF on a Hall thruster [6] under normal operating conditions. Time coherence is reached by applying a potential modulation on a small electrode located near the cathode exhaust. Resonance can be reached by tuning the modulation frequency. This system does not modify the thruster mean behaviour [6]. It is believed that such a technique could be used on many discharges to perform time-resolved measurements when coherence is required.
In this contribution we focus our study on the electric field oscillations by means of TR-LIF measurements on the Xe^+ ion population associated with an active stabilisation of the discharge and with a photon-counting technique. The LIF technique allows a direct measurement of the Ion Velocity Distribution Functions (IVDF) along the laser beam. The IVDF have been acquired along the channel axis with a 200 μm axial resolution. Experiments have been carried out in the discharge of a 200 W permanent magnets Hall thruster at a constant discharge voltage of 200 V and an anode mass flow rate of 1.0 mg/s [7]. The so-called $2S_0$ geometry has been used (the channel width is increased twice compared to a standard design) with BN-SiO_2 channel walls. The background pressure has been kept under 7.10^{-5} mbar-N_2 during operation. The discharge current fluctuations are consistent with those of a Hall thruster operating under standard flight conditions. To our knowledge, this is the first time that natural oscillations of the electric field inside and outside a Hall thruster are recorded. Section II describes the optical bench and the collection technique. The modulation system which allows the oscillation control is also introduced. The third part of this paper is structured as follows. Some time-averaged quantities are presented in Subsec. A. The time-resolved data signal processing technique is described in Subsec. B .The time evolution of the IVDF is given in Subsec. C. Subsection D reports on variation over time of the electric field. Finally, conluding remarks are drawn in Sec. IV.

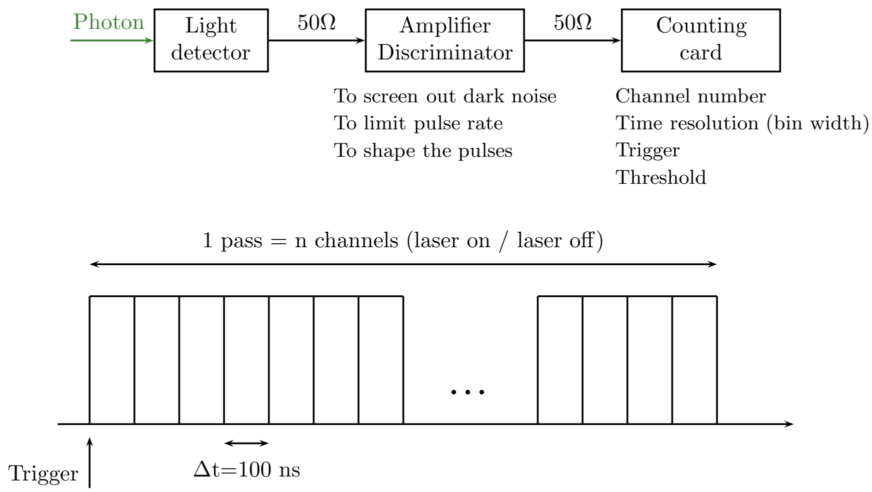

Figure 1. Schematic of the detection branch. Photon events are amplified and selected depending on their energies. The counting card accumulates the events over n channels of 100 ns length each. Both laser-on and laser-off acquisitions are performed to screen out the noise and reveal the fluorescence.

II. Diagnostic technique

A. Optical bench and collection branch

The LIF optical assembly is described in details in a review paper [8]. The $5d^4F_{7/2} \rightarrow 6p^4D_{5/2}$ transition of the Xe^+ ion is probed by an amplified tunable single-mode external cavity laser diode at 834.72 nm. The wavelength is accurately measured by a 60 m/s precision wave meter. A high finesse Fabry-Perot interferometer is used to check the laser stability and detect mode-hops. An anamorphic prism circularizes the laser beam and maximize the transmission through the optical fiber. The laser beam propagates along the thruster axis and is aligned with the center of the discharge channel. The laser typical power density is 10 mW/mm^2 within the measurement volume, which warrants a good signal-to-noise ratio and a limited saturation of the transition.

A collection branch made of a 40 mm focal lens focuses the light onto a 200 μm core diameter optical fiber. Spatial resolution in the axial direction is 200 μm. The fluorescence light is focused onto the entrance slit of a 20 cm focal length monochromator that isolates the 541.9 nm line from the background light. A photomultiplier tube serves as a light detector.

B. Photon-counting technique

The photon counting technique has been applied in the past to diagnose oscillating and pulsed discharges, see papers [9, 10]. However, so far it has never been used on a remotely stabilized discharge. Photons are detected by means of a high gain low dark noise PMT. The detection branch is sketched in Fig. 1. A fast amplifier and discriminator module is used to screen out the noise from the PMT. This has two advantages. First, the count rate is limited to avoid the pulse counter saturation. Second, any single event is converted into a TTL signal. In order to properly adjust the discriminator threshold, events are classified depending on their intensity. Each photon pulse can be distinguished from the background noise by appropriate setting of the discriminator threshold.

The pulse counting device is a multichannel scaler composed of 65535 channels. The entire period of the oscillation can therefore be recorded instead of being reconstructed by an external device over several oscillation periods. Moreover, any wave shape can be recorded with this technique. A modulation-related trigger starts the acquisition of the incoming photon events over a few oscillations period, which warrants perfect reproducibility for each pass. The channel width (the temporal resolution) is 100 ns. Hundreds of thousands of passes are necessary to obtain a good LIF signal-to-noise ratio. For each velocity group

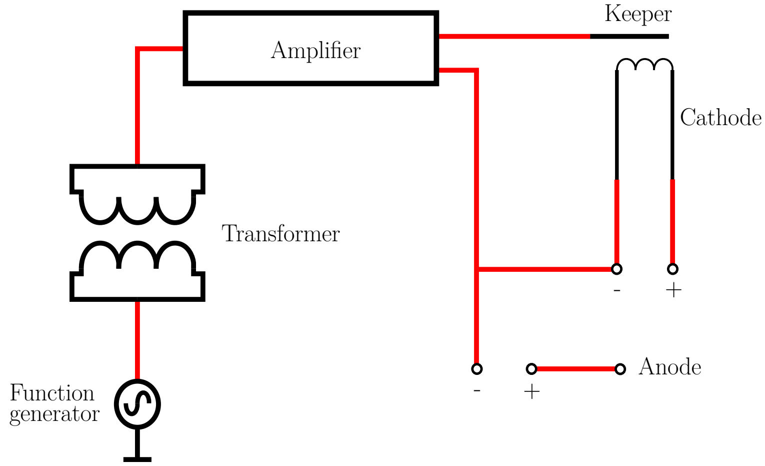

Figure 2. Electrical set-up of the keeper modulation.

measurement, the laser wavelength is kept constant through a feedback loop. The LIF signal is extracted through two successive laser-on and laser-off measurements. The subtraction reveals the fluorescence events collected by the pulse counting device. The statistics is optimized when the subtraction is operated after each pass.

C. Active control method of the discharge oscillations

At low-pressure, i.e. in low density discharges, the recorded fluorescence signal consists of just a few photons per oscillation period. Even if the fluorescence light events can be increased by working in a strongly saturated regime, it appears necessary to realize a statistical accumulation. A temporal coherence of the oscillations is therefore required to perform such an accumulation.

In order to achieve TR-LIF in a Hall thruster, the discharge needs to be maintained in a periodic oscillation regime. The active harmonic system presented here has two main advantages: first, the modulation signal can be used as a trigger signal. Second, the frequency content is fairly the same at any time, which warrants reproducible measurements conditions. An other possibility to actively perform TR-LIF is to use a fast power switch. However, it has been shown that unlike the technique presented here, the power switch perturbs the discharge behavior [5]. Passive systems such as phase sensitive detection time-synchronized on a particular level of the discharge current have been used to extract time-resolved fluorescence signal [11]. This method as well as the one described here (photon counting) is not dependent upon the frequency of the recorded signal and can therefore be applied to many situations. However our stabilizing technique warrants a constant frequency content during operation. Such conditions cannot be obtained through a passive detection.
In order to control the oscillations, a sinusoidal frequency-tunable potential is applied between a floating electrode in the vicinity of the cathode (referred to as the keeper) and the negative pole of the cathode. A schematic view is presented in Fig. 2. The modulation frequency cannot be choosen randomly but corresponds to a resonance of the system. The discharge current oscillation amplitude is monitored as the frequency is adjusted in order to maximize the plasma response to the excitation. The current driven through the keeper is relatively low and represents less than 10% of the discharge current. Such a modulation has been used to perform probe measurements in the far-field plume of Hall thrusters [12].

The resonance with the breathing mode occurs over a 2 kHz band. The monitoring of the maximum discharge current amplitude enables to properly calibrate the modulation frequency. Figure 3 shows the effect of the modulation system on the discharge current. The modulation is set to 16.5 kHz. First it is clear that the mean value of the discharge current remains unchanged, which is mandatory to keep the same thruster average behavior. Second, the discharge current amplitude is clearly higher with the modulation. Although it does not appear on a single screenshot, the ensemble averaging over mulitple acquisitions show a constant time-averaged amplitude. Third, the discharge current phase is constant, which ensures temporal coherence between each measurement pass. The frequency content of the discharge is given by its FFT. The

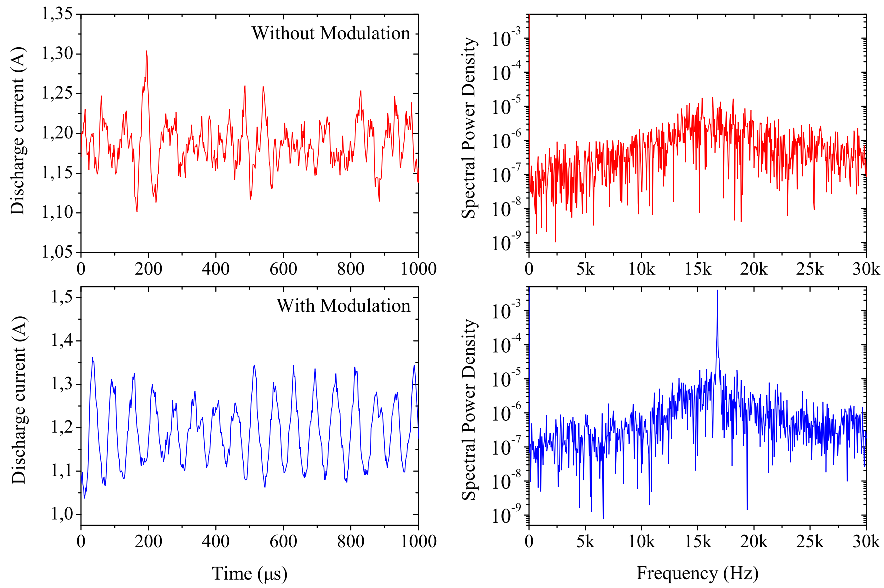

Figure 3. Discharge current with and without the keeper modulation. The modulation frequency is 16.5 kHz.

same harmonic structures exist with and without the modulation except at a particular frequency which corresponds to the modulation one. It is worth noticing that the spectral power density remains unchanged elsewhere. The average modulated discharge current frequency is equal to that of the modulation. The same evolution of the cathode potential relative to ground has been observed. The current driven through the keeper is about 60 mA which corresponds to 5 W injected into a 200 W system. The possibility of modulating the discharge is related to the ratio of the input power of the modulation amplifier to the power of the system to be modulated. A value of 10% enables efficient control and does not disturb the thruster average behavior (see Sec. A). A similar modulation system has been successfully built and tested on a 1.5 kW Hall thruster. In order to achieve proper control upon the breathing mode, a higher amplification was necessary in this case. Similar characteristics of the plasma parameters were observed, meaning this technique is sizeable.

III. Results and discussion

A. Time-averaged quantities

1. Influence of the modulation system

In order to validate the use of the oscillations control to perform TR-LIF, time-averaged LIF (TA-LIF) has been performed with and without the modulation. TA-LIF in Hall thrusters has been extensively described in previous studies [7] and is based on a phase-sensitive detection instead of a photon counting technique. Figure 4 shows the IVDF obtained with and without use of the modulation system. The spectra match each other at almost all velocities. One notices a slight difference on the low velocities part of the main peak. The velocity gap is however close to the measurement error. The discrepancy likely originates from the thruster thermal drift.

2. Comparison with TA-LIF

TA-LIF profile can be reconstructed from the time-resolved measurements. This is a possible way to determine wether the statistical accumulation is good enough to obtain the LIF signal. Figure 5 presents the reconstruction of the time-averaged IVDF from the time-resolved data. The blue line is the raw TA-LIF profile obtained with a lock-in detection technique. The temporal mean of each time-varying velocity group (in red squares) perfectly match the time-averaged measurements, which validates our approach. Several

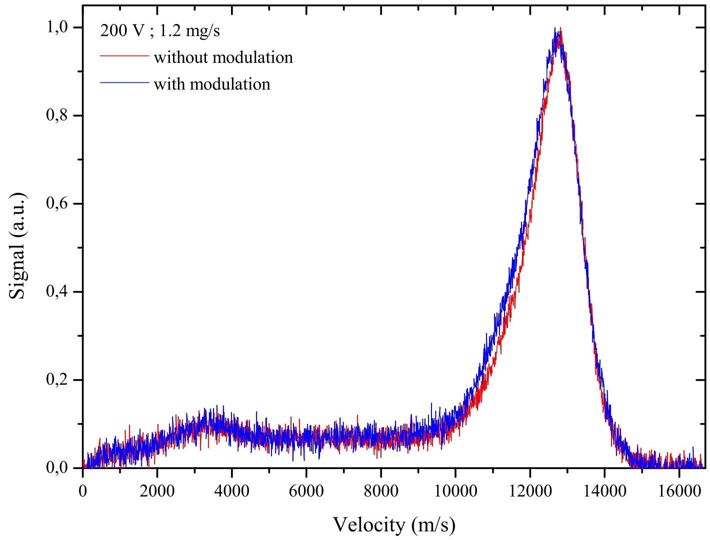

Figure 4. Time-averaged IVDF with and without the modulation system at 5 mm downstream the thruster exit plane.

positions have been examined inside and outside the discharge channel. At each position, a perfect agreement between time-resolved and time-averaged LIF has been observed.

3. Electric field distribution

Most of Hall thruster geometries are based on a constant h/d ratio [1,7], where h is the channel width and d the channel mean diameter. This ratio is thereafter referred to as the standard ratio.
It has been shown that the electric field profile along the channel axis can depart from a single peak located near the maximum of the radial magnetic field [13,14]. In the studies reported by Raitses [14] with emissive probes and by Hargus [13] with both LIF and emissive probes, the electric field ditribution may consists of one or two maxima located inside and outside the channel depending on the experimental conditions. For the standard h/d ratio, the number of extrema depends on the thruster operating point [13]. At a nominal operating point, one electric field maximum is observed for a narrow channel while an enlarged one leads to a split of this peak into two smaller ones [5,14]. The same characteristic can be observed in Fig. 6 where time-resolved IVDF have been time-averaged to compute the mean electric field $\bar{E}$ according to the energy conservation equation. The electric field reads as Eq. (1)

$$\bar{E} = \frac{m_{\mathrm{i}} < \bar{v_z} >}{e} \frac{d < \bar{v_z} >}{dz} \tag{1}$$

where m_{i} is the ion mass, e is the elementary charge and $< \bar{v_z} >$ is the time-averaged ion mean velocity along the channel axis (first moment of the IVDF). The electric field is generated by a sharp potential drop due to the high plasma resistivity in the strong magnetic field region. Electron diffusion therefore controls the electric field shape and position. Two regions are well defined in terms of transport. The exit plane represents a border between them. Two possibilites to account for this observation can be drawn. First, two different mechanisms could dominate inside and outside the channel. We could for instance suppose that the plasma/wall interactions control the transport inside the channel while the high-frequency microturbulence acts outside. The two mechanisms may also appear together with a varying amplitude along the channel. Second, the hypothesis of an outside production zone can be made. However, the time-averaged axial ion density profile is not composed of two peaks but of one large peak extending from - 6 mm inside the channel to 8 mm outside.

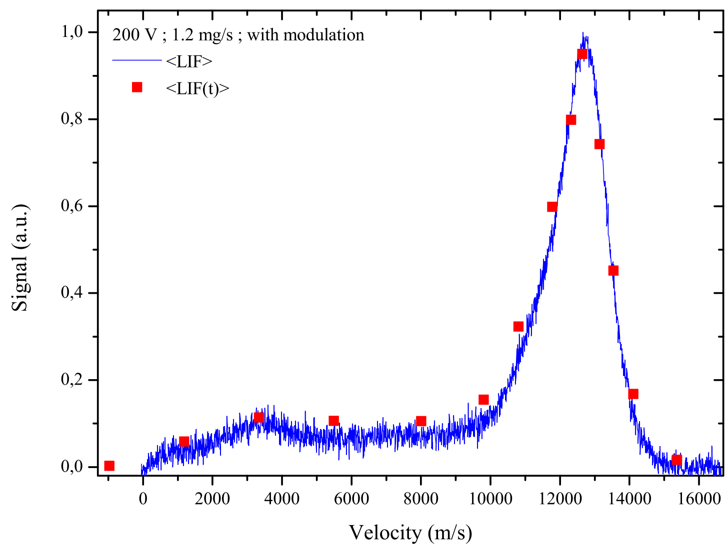

Figure 5. Comparison between the IVDF obtained by time-averaged measurements and the IVDF inferred from photon counting at 5 mm downstream the thruster exit plane.

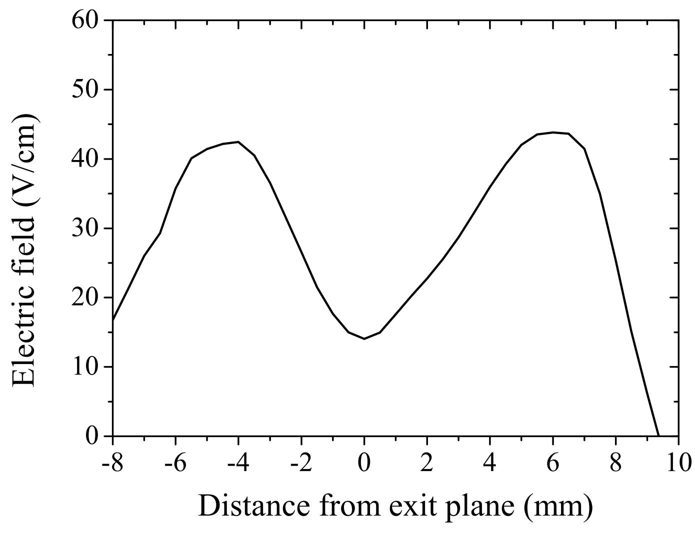

Figure 6. Temporal mean of the axial electric field along the discharge channel.

B. Signal analysis method of the time-resolved data

Each IVDF is renconstructed from 15 ion velocity time-series which exhibits a strong non-stationary behavior. The Hilbert-Huang analysis has therefore been used instead of the classical Fourier decomposition to post-process the time-resolved data. The Hilbert-Huang process consists of applying the Empirical Mode Decomposition (EMD) technique [15] (the Huang sifting process) to the time-series of the ion velocity and to use the Hilbert transform to perform the spectral analysis [16, 17] of the generated modes, the so-called Intrinsic Mode Functions (IMF). The EMD method is well-adapted to the study of non-stationary signals. The usual techniques, such as the Fourier or the wavelet analyses, presuppose the decomposition functions of the signal to be analyzed. The Hilbert-Huang decomposition self-generates the IMF. The Hilbert spectral analysis gives the instantaneous amplitude, phase and frequency of each mode. The spectral content of the original signal is then determined at each time. By integrating the Hilbert spectrum over time, it is possible to compute the marginal spectrum of the decomposition, which corresponds to the Fourier spectrum in the Fourier analysis.

Figure 7 presents the EMD applied to the signal recorded at z=-8mm inside the channel for the most probable ion velocity group. The IMF averaged frequencies range from the kHz up to the MHz. Three families of plasma oscillations dominate the decomposition outcome. The breathing mode is given by IMFs 8 to 10 (averaged frequencies ranging from 1 kHz to 40 kHz). The IMFs 4, 5 and 6 whose frequencies range from 100 to 600 kHz may correspond to the ion transit time oscillations. The last family is composed by IMFs 1, 2 and 3. Their averaged frequencies are above 1 MHz. The pulse-counting card acquisition frequency being 10 MHz, these last three IMFs are not considered in our analysis. The seventh IMF mean frequency is around 65 kHz. This frequency area will be further investigated, and may correspond either to a density gradient-driven instability that is peculiar to weakly ionized plasmas or to an ionization-type instability [18].

C. Time evolution of the IVDF

The ion velocity distribution functions have been measured along the center of the discharge channel from - 8 mm to 10 mm, 0 mm being the exit plane. The channel axis is referred to as the z axis.
Figures 8(a) and 8(b) shows a typical IVDF measurement. The ion velocity is plotted against time at two different locations along the channel axis. The colourbar gives the number of fluorescence photons accumulated over the acquisition. Two frequency bands can be distinguished: a low frequency group until 30 kHz and higher groups at hundreds of kHz. All the measured IVDF oscillate at the breathing mode frequency. It is easily observable in Fig. 8(b) that different velocity groups can be phase shifted between each other in a given IVDF.

The Hilbert spectral analysis of a time-series generates an object called the marginal spectrum. This spectrum is comparable to the Fourier spectrum when using the FFT technique. However, the marginal spectrum interpretation is enhanced compared to the Fourier spectrum by the combination of the powerful non-stationary modal decomposition and of the Hilbert analysis of the modes. Four marginal spectra are given in Fig. 9. The spectral amplitude is plotted against the frequency in MHz. These spectra correspond to the analysis of the most probable velocity ion group of the IVDFs from z = - 6 mm to z = - 3 mm inside the channel. The low frequency part of the discharge (around 30 kHz) carries most of the spectral energy. It is the well-known breathing mode. High frequencies appear on the frequency spectrum whereas only the breathing mode has been stabilised by the modulation system, meaning that higher frequency phenomena are breathing mode dependent. It is indeed meaningful to remind that the LIF signal needs to be accumulated over many oscillation periods to be screen out from the noise. Since the LIF acquisitions are triggered on the discharge modulation which occurs at $\sim$ 15 kHz, high frequency modes may not appear, unless they have a phase which does not vary during the acquisition (typically around 5 min). Therefore, it can be said that the high frequency groups shown by arrows on the marginal spectra in Fig. 9 are stabilized by the breathing mode. These frequencies are consistent with the theoretical frequencies for the ion transit time oscillations calculated at this operating point. It can be noticed that the would-be ion transit time instability frequency shifts towards the high frequency side when moving along the channel axis. Finally, part of the energy is located in the frequencies around 100 kHz. These frequencies may be associated to gradient instability or to electron-neutrals collisions as mentioned in III B.

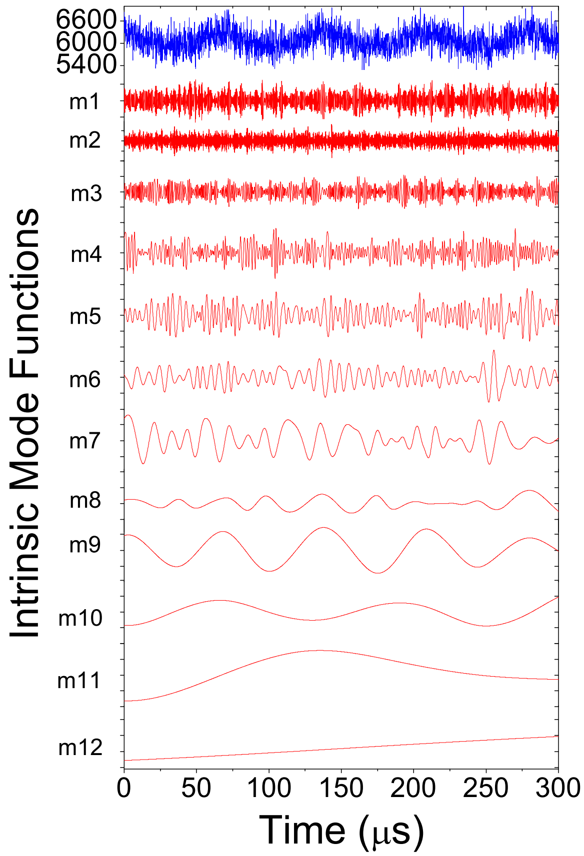

Figure 7. EMD technique applied to the analysis of the ion most probable velocity group time-series at z=-8 mm. The original signal (blue) is plotted in fluorescence photons against time. The modes (red) are plotted in arbitrary units against time.

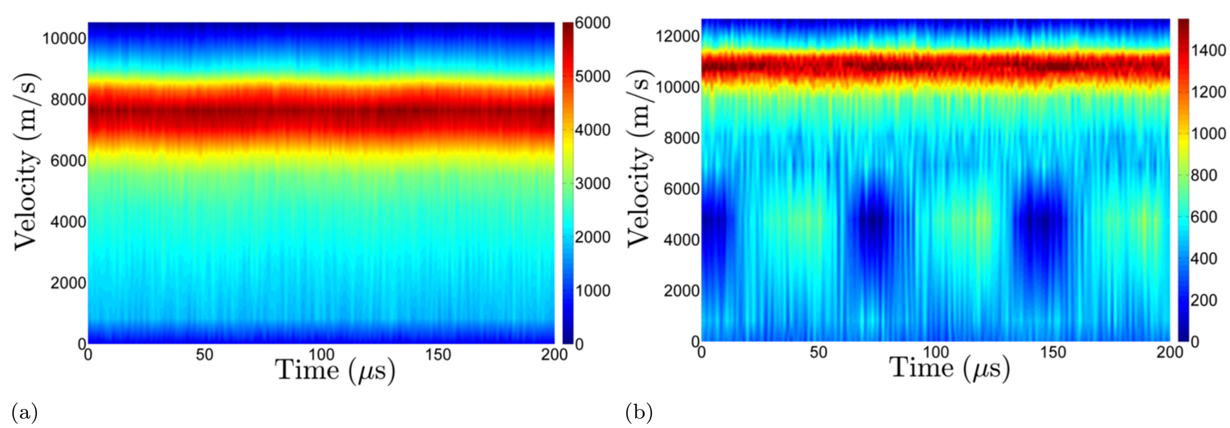

Figure 8. Time evolution of two IVDF both inside and outside the thruster channel (raw traces): (a) shows the IVDF at 3 mm inside the channel; (b) presents the IVDF at 4 mm away from the exit plane.

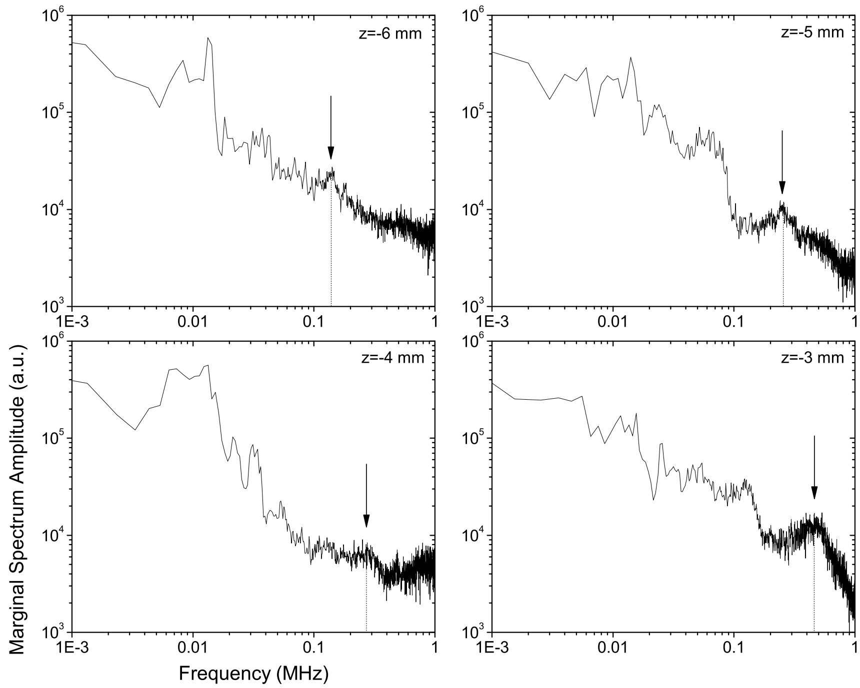

Figure 9. Marginal spectra associated with the ion most probable velocity group time-series at four different locations inside the channel. High frequency groups stabilized by the breathing mode are designated by arrows.

D. Time evolution of the electric field

The time-resolved electric field has been computed from the IVDF. An appropriate method consists of using the equation of motion for unmagnetized ions [5]. The axial component of the electric field reads as Eq. (2)

$$E_z = \frac{m_{\rm i}}{e}\left(\frac{\partial \bar{v_z}}{dt} + \bar{v_z}\frac{\partial \bar{v_z}}{dz}\right) \tag{2}$$

where $\bar{v_z}$ is the ion mean velocity at a given position along the discharge channel axis and at a given time. The ion pressure term can be neglected under the assumption of cold ions.

1. Low-frequency oscillations

Figure 10 shows the time evolution of the accelerating field both inside and outside the channel. The field is plotted as a function of space and time. The z coordinate stands for the distance from the exit plane. The two peaks structure is clearly seen and a phase shift of almost π between the two peaks is visible. The oscillation amplitude inside the channel is weak compared to the amplitude of the second peak, as illustrated in Fig. 10. Since the discharge voltage is constant, the outside electric field is widening when diminishing to satisfy

$$U_{\rm acc} = \int_{channel} E_z(z,t)dz = \text{ constant } \forall t \tag{3}$$

It has been verified that U_{acc} = 140 V at each time. This potential is lower than the applied discharge voltage since one must consider the cathode potential relative to the ground (-20 V), the losses in the system and the lower tail of the IVDF which lowers the overall accelerating potential.

The evolution of the electric field has been plotted against the distance from the exit plane in Fig. 11 for four different instants during a breathing oscillation. A discharge current oscillation period is also shown to associate the electric field profile with the current evolution. The internal electric field peak does not move in space and changes slightly in amplitude, while the external one varies from 43 V/cm at 4 mm to 55 V/cm at 7 mm downstream the exit plane. The peak inside the channel is increasing in intensity as

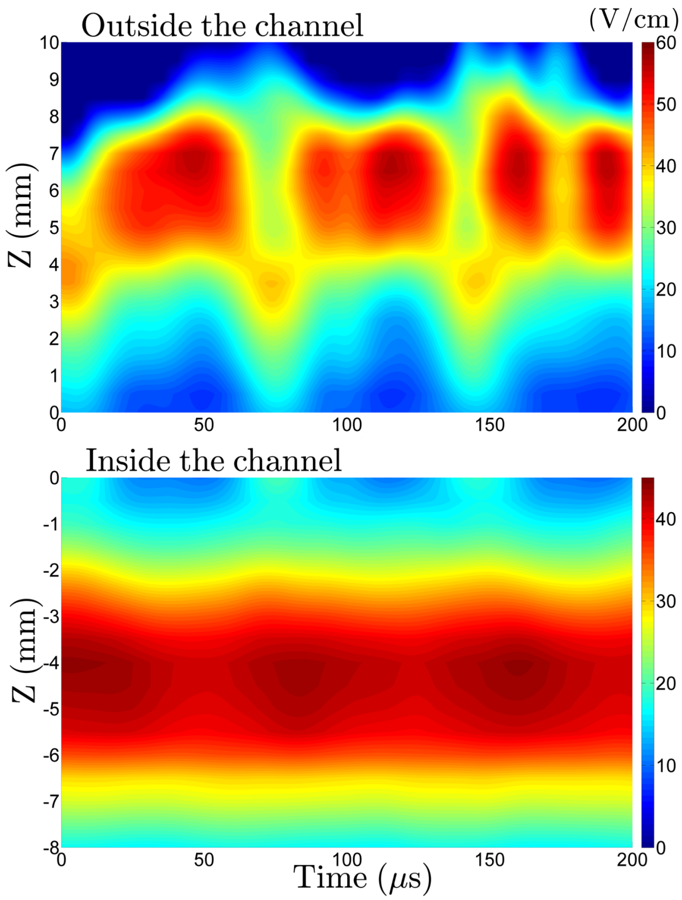

Figure 10. Time evolution of the electric field axial component along the discharge channel. Colourbars have been adjusted inside and outside the channel to correctly reveal the oscillations.

expected when the discharge current oscillation is rising.
These results do not reveal an electric field wave propagating in space unlike the previous measurements performed on a larger thruster [5]. However, several differences may explain this behavior. First the channel geometry is not the same. A larger h/d ratio is used here instead of the standard one. Second, the temporal coherence is obtained here through an active modulation of the discharge current that does not modify the thruster mean behavior [6] while the past study used a fast power switch to induce strong oscillations [5]. This system has been shown to change the averaged characteristics of the discharge and a higher discharge current oscillation could generate a wave as the thruster is igniting at each cycle [14].

A characteristic of the breathing oscillations is the back and forth motion of the ionization zone. This leads to a periodic increase in ion density outside the discharge channel. The concomitant electric field can be computed from these variations. Quasi-neutrality can be supposed since the characteristic length of the density gradients is much above the Debye length. We also assume a purely radial magnetic field along the discharge channel axis between $z = 0$ mm and $z = 10$ mm. The linearized equation of motion for the magnetized electrons reads

$$m_e \frac{\partial V_{e,z}}{\partial t} = -eE_z - \frac{\nabla p_e}{n} + eV_\theta B_r \tag{4}$$

The left-hand side term of Eq. (4) can be neglected owing to the low electron mass. Thus the axial electric field is given by

$$E_z = V_\theta B_r - \frac{kT_e}{e}\frac{\nabla n}{n} \tag{5}$$

The corresponding electric field is shown in Fig. 12. The electric field computed by this approach is in

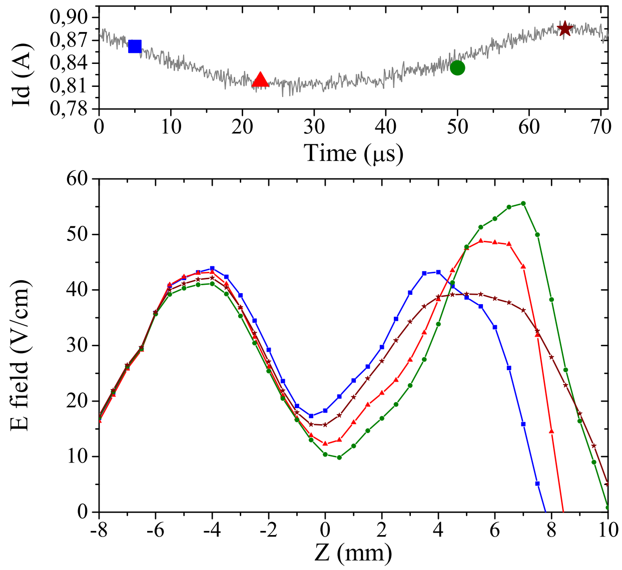

Figure 11. Time evolution of the electric field along the discharge channel at t=5 µs, 22 µs, 50 µs and 65 µs.

good agreement with the electric field directly computed from the measurements with $V_\theta = 400$ km/s, $B_r = 0.015$ T and $T_e = 25$ eV. The outside peak of the electric field is therefore attributed to electron density fluctutations generated by the back and forth motion of the ionization zone. The stability of the electric field inside the channel indicate that the ionization zone does not strongly oscillate at the breathing mode in this area.

2. High-frequency oscillations

We have demonstrated in Subsec. C that part of the high frequency content of the ion velocity can be stabilized by the breathing mode modulation. It is possible to compute the time-evolution of the electric field by selecting the contribution of the high frequency IMFs given by the EMD. The high frequency evolution of the electric field is given in Fig. 13(a) and 13(b). The electric field is plotted as a function of space and time. Time scales have been adjusted to the displayed frequency range. The colorbar unit is in V/cm. Figure 13(a) displays the electric field frequency content between 100 kHz and 400 kHz. Figure 13(b) displays the electric field frequency content between 400 kHz and 900 kHz. The electric field exhibits strong oscillations over the entire studied high frequency range. To the best of our knowledge, these results are the first time direct evidence of the electric field oscillations within a frequency range that corresponds to the ion transit time oscillations of the discharge. Figure 13(b) shows that the electric field is propagating towards the anode. The wave front velocity is propagating at a velocity of 4.35 km/s.

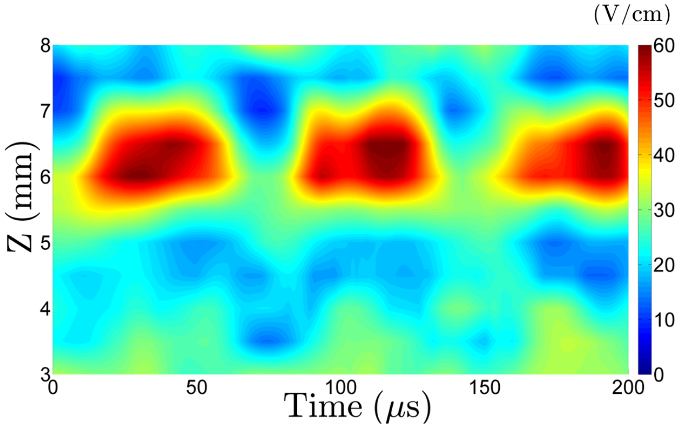

Figure 12. Time evolution of the electric field inferred from the density fluctuations (to be compared with Fig. 10).

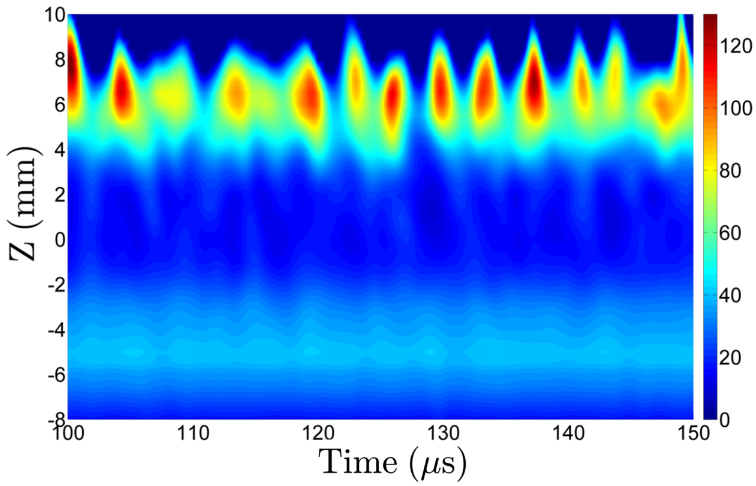

(a)

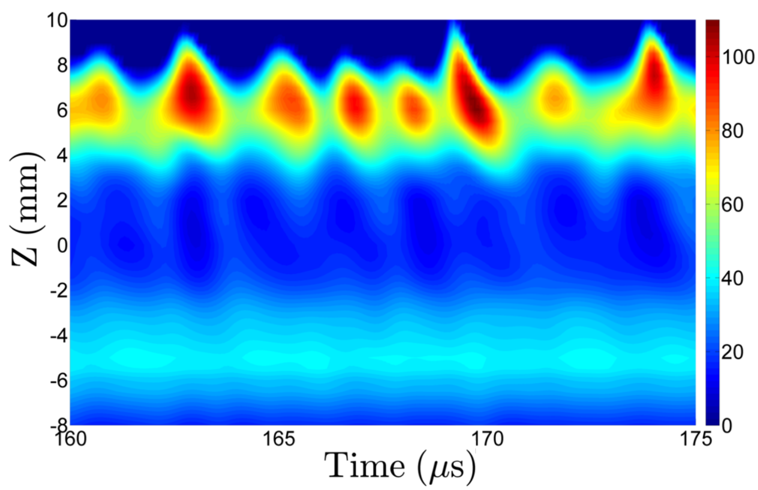

(b)

Figure 13. Time evolution of the high frequency content of the axial electric field along the channel axis: (a) frequencies between 100 kHz **and 400** kHz**; (b) frequencies between 400** kHz **and 900** kHz**. Colorbars are in** V/cm**.**

IV. Conclusion

The examination of the temporal characteristics of a Hall thruster discharge has been performed by means of TR-LIF spectroscopy. Several results are of great interest. First, the photon-counting technique is shown to be valid as a diagnostic technique provided the discharge oscillations can be maintained in a quasi-harmonic regime. Second, we have demonstrated the possibility to actively control the low frequency oscillations by means of a potential modulation on a floating electrode, without change of the plasma mean behavior. The association of both the modulation and the TR-LIF techniques appears to be very effective to obtain time-resolved data.

Time-resolved measurements of the ion velocity distribution functions along the discharge channel of a Hall thruster have been used to compute the time evolution of the electric field in this propulsion device. The low and high frequency electric field exhibits strong oscillations outside the channel. The low frequency oscillations are associated with the breathing mode (ion density fluctuations) while internal electric field oscillations are almost non-existant. The breathing oscillations induced by the modulation system are consistent with the normal operating conditions of a Hall thruster. High frequency oscillations are visible on the IVDF and on the accelerating electric field. These high frequency evolutions indicate that the ion transit time instability occurs at this operating point. We have also demonstrated that these frequency modes are influenced and even stabilized by the low frequency oscillations.

Acknowledgments

J. Vaudolon benefits from a CNES-Snecma Ph.D. grant.

References

[1]K. Dannenmayer and S. Mazouffre. Elementary scaling relations for Hall effect thrusters. *J. Propul. Power*, 27:236, 2011.

[2]H.R. Kaufman V.V. Zhurin and R.S. Robinson. Physics of Closed Drift Thrusters. *Plasma Sources Sci. Technol.*, 8:R1, 1999.

[3]EY. Choueiri. Plasma oscillations in hall thrusters. *Phys. Plasmas*, 8:1411, 2001.

[4]D Staack, Y Raitses and N J Fisch. Investigations of Probe Induced Perturbations in a Hall Thruster. Paper 2002-4109, Proc. 38th AIAA/ASME-/SAE/ASEE JPC, Indianapolis, IN, 2002.

[5]S. Mazouffre and G. Bourgeois. Spatio-temporal characteristics of ion velocity in a hall thruster discharge. *Plasma Sources Sci. Technol.*, 19(065018):9, 2010.

[6]J. Vaudolon, L. Balika and S. Mazouffre. Photon counting technique applied to time-resolved laser-induced fluorescence measurements on a stabilized discharge. *Rev. Sci. Instrum.*, 84(073512), 2013.

[7]G. Bourgeois S. Mazouffre M. Guyot A. Lejeune, K. Dannenmayer and S. Denise. Ionization and acceleration processes in a small, variable channel width, permanent-magnet hall thruster. *J. Phys. D: Appl. Physics*, 45(185203), 2012.

[8]S. Mazouffre. Laser-induced fluorescence diagnostics of the cross-field discharge of Hall thrusters. *Plasma Sources Sci. Technol.*, 22(063001), 2013.

[9]B. Pelissier and N. Sadeghi. Time-resolved pulse-counting lock-in detection of laser induced fluorescence in the presence of a strong background emission. *Rev. Sci. Instrum.*, 67(3405), 1996.

[10]D. Gawron S. Mazouffre and N. Sadeghi. A time-resolved LIF study on the ion velocity distribution function in a Hall thruster after a fast current disruption. *Phys. Plasmas*, 16(043504), 2009.

[11]M.A. Capelli N.A. MacDonald and W.A. Hargus. Time-synchronized continuous wave laser-induced fluorescence on an oscillatory xenon discharge. *Rev. Sci. Instrum.*, 83(113506), 2012.

[12]M. Tichy K. Dannenmayer, P. Kudrna and S. Mazouffre. Time-resolved measurement of plasma parameters in the far-field plume of a hall effect thruster. *Plasma Sources Sci. Technol.*, 21(055020):9, 2012.

[13]W A Hargus Jr. and M A Cappelli. Interior and exterior laser-induced fluorescence and plasma measurements within a hall thruster. *J. Propul. Power*, 18:159–168, 2002.

[14]M Keidar Y Raitses, D Staack and N J Fisch. Electron-wall interaction in hall thrusters. *Phys. Plasmas*, 12(057104), 2005.

[15]S. R. Long M. C. Wu H. H. Shih Q. Zheng N.C. Yen C. C. Tung N. E. Huang, Z. Shen and H. H. Liu. The empirical mode decomposition and the hilbert spectrum for nonlinear and non-stationary time series analysis. volume 454 of *Proc. R. Soc. London*, pages 903–955, 1998.

[16]Z. Shen N. E. Huang and S. R. Long. A new view of nonlinear water waves: The hilbert spectrum. *Annu. Rev. Fluid Mech.*, 31:417–457, 1999.

[17]J. Kurzyna, S. Mazouffre, A. Lazurenko, L. Albarde, G. Bonhomme, K. Makowski, M. Dudeck and Z. Peradzynski. Spectral analysis of hall-effect thruster plasma oscillations based on the empirical mode decomposition. *Phys. Plasmas*, 12(123506), 2005.

[18]E.Y. Choueiri. Characterization of oscillations in closed drift thrusters. paper AIAA-94-3013, 30th Joint Propulsion Conference, Indianapolis, IN, 1994.